Journal of Low Temperature Physics (2024) 216:264–272
https://doi.org/10.1007/s10909-024-03130-0

Thermal Annealing of AlMn Transition Edge Sensors for Optimization in Cosmic Microwave Background Experiments

Benjamin Westbrook[1] · Bhoomija Prasad[1] · Christopher R. Raum[1] · Adrian T. Lee[1] · Aritoki Suzuki[2] · Johannes Hubmayr[3] · Shannon M. Duff[3] · Micheal J. Link[3] · Tammy J. Lucas[3]

Received: 28 November 2023 / Accepted: 6 April 2024 / Published online: 8 June 2024

Abstract

The 2020 decadal review recognized the measurement of the polarization of the cosmic microwave background (CMB) to be a top priority for the decade. CMB experiments including POLARBEAR2/Simons Array, Atacama Cosmology Telescope/Advanced-ACT, SPT-3G, the Simons Observatory, and CMB-S4 have or will use transition edge sensor (TES) bolometer fabricated with Aluminum doped with Manganese (AlMn). AlMn is a popular material choice as the superconducting transition temperature (T_c) and normal resistance (R_n) of the TES can be tuned with Mn concentration, geometric patterning, film thickness, and thermal annealing. In addition the conductivity is appropriate for both time division multiplexing and frequency division multiplexing that require 10 mΩ and 1 Ω sensors respectively. In this paper we present work on the ability to tune the T_c of a film based on its time and temperature thermal tuning profile combined with room temperature monitoring of film resistivity. Such control allows for the fabrication of a wide range of TES parameters from a single AlMn concentration. Scanning electron microscope (SEM) imaging shows that the AlMn film's grain boundaries are changed by thermal annealing making the film more conductive and raising its superconducting transition temperatures, and that at high enough temperatures will eventually recover the T_c of bulk Al. We find that baking films at ~ 200 °C for tens of minutes yields a T_c that is suitable for 100 mK base temperature experiments and we present on the thermal tune profiles of several different thicknesses of AlMn.

Keywords Cosmic microwave background · Transition edge sensor · Bolometer · Polarization · Readout · Cryogenics · AlMn

Extended author information available on the last page of the article

1 Introduction

Transition edge sensors (TESs) have been the preferred type of low temperature detector for cosmic microwave background (CMB) experiments for over a decade for three primary reasons [1–5]. First, the sensitivity of most CMB TESs is well below the background noise levels from the background of photons in the telescope. Secondly, they are lithographically fabricated on 150 mm silicon wafers, which provides excellent uniformity across a given detector array with $\sim$ 1000 TESs. Finally, the normal resistance of the TES are compatible with multiple types of cyrogenic multiplexing making this technology scalable to experiments with many tens to hundreds of thousands of detectors [4, 5].

When constructing a TES bolometer the following design choices must be satisfied: (1) most of the TESs have the desired critical superconducting transition temperature (T_c) within a specified range, (2) the TES must have the appropriate normal resistance (R_n) both above T_c and in operation, (3) the properties of the TESs (T_c and R_n) are uniform across the wafer, and (4) the TESs properties do not vary from wafer to wafer across multiple fabrication runs. Aluminum doped with Manganese (AlMn) has emerged as top candidate for the production of TES bolometer arrays for CMB polarization experiments [2–7]. Deposition of AlMn is typically performed using state of the art sputter deposition equipment kept under consistently high vacuum providing natural solutions to criteria (3) and (4). [8, 9] The manganese concentration is typically just a few tenths of a percent (either by weight or atomic percentage) and these films have resistivities very close to that of aluminum. In our work, we present TESs films that have normal and operational resistances ranging from 6 mΩ to 1.2 Ω, which are appropriate for time domain multiplexing, microwave squid multiplexing, and frequency domain multiplexing [3, 4, 6] which is a solution to criteria (2). Most importantly, we discuss the ability to tune the T_c of a AlMn film to the specification of a given experiment. The T_c of AlMn films depends on many things including but not limited to: manganese concentration, film thickness, thermal annealing temperature (T_{anneal}), thermal annealing time (t_{anneal}), and device geometry. We present our recent work on tuning AlMn films and the methods we use to modulate the T_c and R_n of a TES for all types of modern CMB polarization experiments.

2 Methodology

In this work, we fabricated and tested two types of devices: (1) singulated dice coated with unpatterned films of thin aluminum manganese and (2) patterned TES with niobium leads (see Fig. 1). The bare films are DC magnetron sputtered coated on to silicon substrates coated with an insulating layer of silicon nitride after an RF sputter-etch cleaning processes. These films are useful for both singulating into dice for cryogenic electrical characterization or kept as whole wafers as ‘witnesses’ to fully patterned TESs.

By contrast, the patterned TESs are constructed by sputter- depositing a layer of AlMn and then patterning the desired base geometry of the TES into the film. A

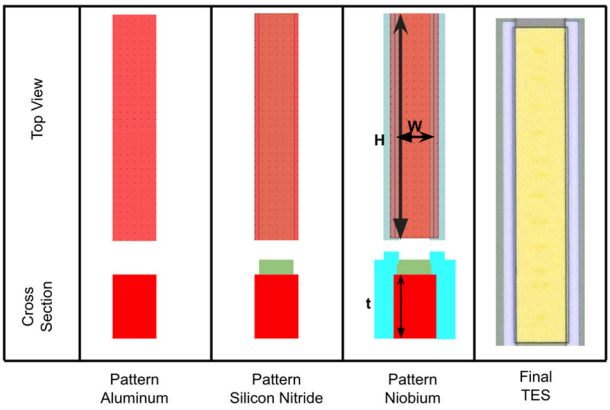

Fig. 1 A diagram of the TES construction stack used in this work. The three left panel have top and cross sectional views. The number of squares (□) in the TES is defined by width (W) of the passivation layer, the height (H) of the AlMn panel as shown in the third panel. The thickness (t) of the TES plays a role in the final T_c and R_n of the device. A photograph of a completed TES is found in the right most panel

passivating layer of silicon nitride is patterned to overlap the AlMn protecting most of the surface but leaving the AlMn edges exposed for contact with an overlapping layer of niobium leads. The interface of the AlMn, the silicon nitride passivation layer, and Niobium combined together define the geometry of the TES as shown in Fig. 1. Note that every time we process a device wafer with patterned TESs we have a corresponding bare film 'witness' wafer to accompany the patterned wafer in future thermal annealing steps. The resisitivity (R_s) of the wafer is measured as function of thermal annealing to compare against the T_c and R_n data coming from the patterned TESs.

3 Phenomenology

In this work, we offer some insight into what is occurring in the bulk of the film, especially, at the grain boundaries that causes the changes to the normal resistance and superconducting transition temperature that we see which are shown in Table 1.

Table 1 A table summarizing the mechanisms one can use to change T_c and/or R_n of AlMn

Tuning mechanism	Value	Impact on T_c	Impact on R_n	Fixed/Variable
Manganese Concentration	5500 ppmw	High	Low	Fixed
TES Width (Nb proximity)	3–25 μm	High	High	Variable
Film Thickness	900 Å or 4000 Å	Med-high	High	Fixed
T_{anneal}	170° C to 230° C	Med-high	Low	Variable
t_{anneal}	1 to 120 min	low-med	Low	Variable

In practice, the geometry and thickness are first used to find the correct R_n and then thermal annealing is used to tune the T_c into specification

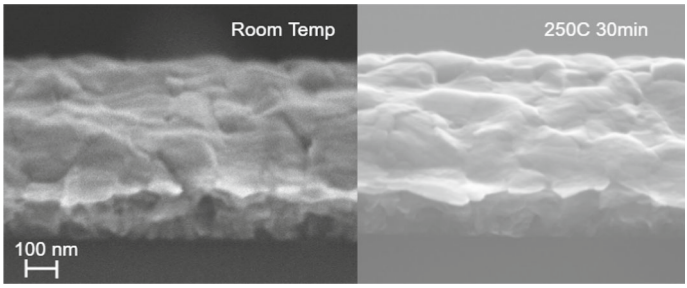

Fig. 2 Left: A SEM image of the grain boundaries on un-annealed film. Right: A SEM image of the AlMn grain boundaries of a film on a sister die from the same wafer annealed to 250° C for 30 min. We observe a softening of the grain boundaries in the annealed sample, which is consistent with other phenomenology and literature [8, 10]

We looked at physical effects of thermal tuning directly using a scanning electron microscope (SEM) as shown in Fig. 2. The most notable difference we find before and after thermal annealing is the softening of the grain boundaries in the film. These changes to the grain boundaries make the AlMn behave more and more like bulk Al as the effect of the Mn on the Al is reduces with further thermal annealing.

4 Parameter Tuning

Ultimately one must be able to fabricate a TES according to the design specifications of a planned experiment. In this section we discuss both the tuning of the R_n and T_c.

4.1 Normal Resistance

In this work, we focused on developing TESs with normal resistance of a ~ 10 mΩ for time division multiplexing (TDM) and microwave SQUID mutliplexing, and 1 Ω for frequency division multiplexing (FDM). UCB has a strong heritage developing 1 Ω sensors for FDM for POLARBEAR-1, the Simons Array and NIST has a strong heritage developing 10 mΩ sensors for ACT, Advanced-ACT, SPIDER, and Simons Observatory [2, 6, 11, 12]. The R_n tuning is achieved by combining thickness (4000 Å vs 800 Å) and TES geometry (0.2 vs 1.8 □) which is shown in Table 2 and Fig. 3.

4.2 Superconducting Transition Temperature

To understand this parameter space we took two primary approaches: (1) to explore the effect of annealing temperature and time vs T_c and (2) to explore the effect of using Nb to proximitize the TES with a higher transition temperature materials. For a constant anneal time (t_{anneal}), the T_c of a AlMn TES will increase with temperature. We generally find monotonic increase with bake temperature, while form a hockey stick shaped curve with a slow rising portion, a 'knee', and then a fast rising portion

Table 2 Summary of all of the TES geometries we fabricated and measured as part of this work

Geometry (μm x μm)	Thickness (nm)	R_n (mΩ)
25 x 200	400	6.0
25 x 160	400	8.0
7 x 11	400	31
10 x 12	400	38
13 x 12	400	42
22 x 12	400	85
25 x 4	400	650
17 x 12	90	975

A range of 6.0 to 975 mΩ was achieved

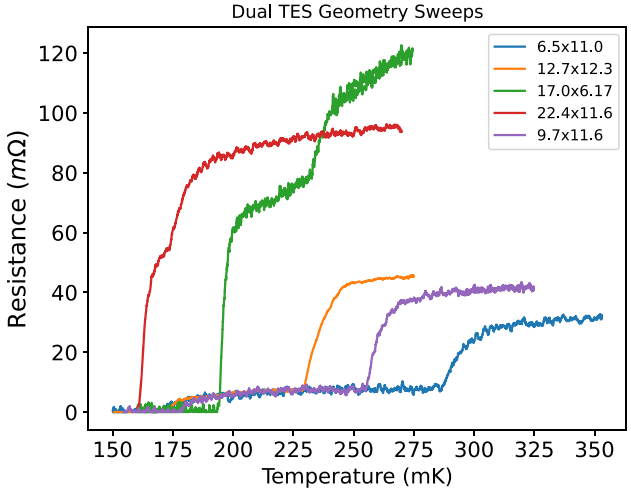

Fig. 3 Five different R vs Temperature curves for different dual TES designs. The transition depends quite strongly proximity effect which is controlled with the spacing of the Niobium leads. This effect makes fabricating TESs with a wide range of both T_c and R_n with a single AlMn thickness possible

of the curve as shown in Fig. 4. Once a baking temperature is fixed and only the time is increased we find the T_c continues to monotonically increase but a diminishing rate. We have developed a strategy to walk up the temperature in 10 min increments until we can measure a T_c above the base temperature of our dilution refrigerator ($\sim$20 mK). At this point one can calculate the slope of that tuning rate and use the pseudo-linear annealing time vs T_c to dial in the desired T_c (see Fig. 4).

5 Conclusion

We presented the general framework to use sputter deposited AlMn to build TESs appropriate for modern CMB experiments. While, a large number of variable can affect the final operating resistance and transition temperature of the TES, we present

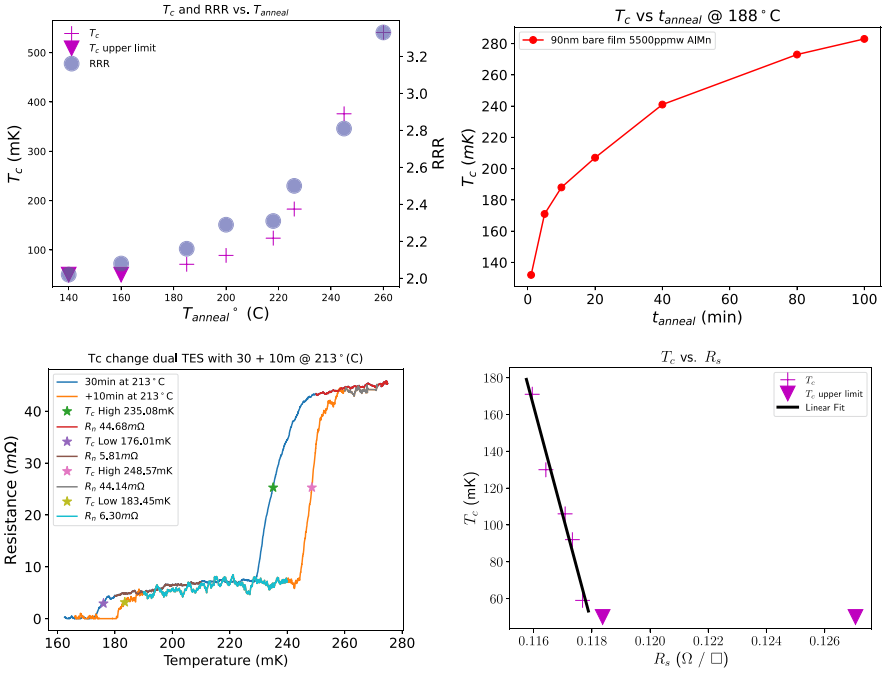

Fig. 4 Top: T_c vs T_{anneal} (left) and T_c vs t_{anneal} (right) and for bare films of AlMn singulated into dice. Bottom Left: The same dual transition TES tested twice with a thermal anneal between cryogenic runs. The T_c increases and the R_n decreases in both transition as expected. Bottom Right: R_s of a witness wafer that was co-thermally annealed alongside the TESs measured in the dilution refrigerator at UC Berkeley

a method to reduce the process to TES geometry and TES thermal tuning using both time and temperature as a control of T_c. In addition, we showed that a dual transition can be constructed using a single layer of AlMn using the niobium leads and TES geometry to create two distinct transitions in the TES. This is particularly useful to use the same TES to characterize the overall pixel performance in the laboratory before deployment for observations.

Acknowledgements We acknowledge the support from the DOE and NSF for work done by UC Berkeley for the CMB-S4 Detector fabrication working group. This work was performed under intra-university transaction agreement No. 7591532. We also acknowledge support in part by the Simons Foundation Award #457687, B.K.

References

1. J.A. Sobrin, A.J. Anderson, A.N. Bender, B.A. Benson, D. Dutcher, A. Foster, N. Goeckner-Wald, J. Montgomery, A. Nadolski, A. Rahlin, P.A.R. Ade, Z. Ahmed, E. Anderes, M. Archipley, J.E. Austermann, J.S. Avva, K. Aylor, L. Balkenhol, P.S. Barry, R.B. Thakur, K. Benabed, F. Bianchini, L. E. Bleem, F.R. Bouchet, L. Bryant, K. Byrum, J.E. Carlstrom, F.W. Carter, T.W. Cecil, C.L. Chang, P. Chaubal, G. Chen, H.-M. Cho, T.-L. Chou, J.-F. Cliche, T.M. Crawford, A. Cukierman, C. Daley, T. de Haan, E.V. Denison, K. Dibert, J. Ding, M.A. Dobbs, W. Everett, C. Feng, K.R. Ferguson, J. Fu, S. Galli, A.E. Gambrel, R.W. Gardner, R. Gualtieri, S. Guns, N. Gupta, R. Guyser, N.W. Halverson, A.H.

Harke-Hosemann, N.L. Harrington, J.W. Henning, G.C. Hilton, E. Hivon, G.P. Holder, W.L. Holzapfel, J.C. Hood, D. Howe, N. Huang, K.D. Irwin, O.B. Jeong, M. Jonas, A. Jones, T.S. Khaire, L. Knox, A.M. Kofman, M. Korman, D.L. Kubik, S. Kuhlmann, C.-L. Kuo, A.T. Lee, E.M. Leitch, A.E. Lowitz, C. Lu, S.S. Meyer, D. Michalik, M. Millea, T. Natoli, H. Nguyen, G.I. Noble, V. Novosad, Y. Omori, S. Padin, Z. Pan, P. Paschos, J. Pearson, C.M. Posada, K. Prabhu, W. Quan, C.L. Reichardt, D. Riebel, B. Riedel, M. Rouble, J.E. Ruhl, B. Saliwanchik, J.T. Sayre, E. Schiappucci, E. Shirokoff, G. Smecher, A.A. Stark, J. Stephen, K.T. Story, A. Suzuki, C. Tandoi, K.L. Thompson, B. Thorne, C. Tucker, C. Umilta, L.R. Vale, K. Vanderlinde, J.D. Vieira, G. Wang, N. Whitehorn, W.L.K. Wu, V. Yefremenko, K.W. Yoon, M.R. Young, The Design and Integrated Performance of SPT-3G. Aapjs **258** (2), 42 (2022). https://doi.org/10.3847/1538-4365/ac374f. arXiv:2106.11202 [astro-ph.IM]

2. BICEP2 Collaboration, Keck Array Collaboration, SPIDER Collaboration, Ade, P.A.R., Aikin, R.W., Amiri, M., Barkats, D., Benton, S.J., Bischoff, C.A., Bock, J.J., Bonetti, J.A., Brevik, J.A., Buder, I., Bullock, E., Chattopadhyay, G., Davis, G., Day, P.K., Dowell, C.D., Duband, L., Filippini, J.P., Fliescher, S., Golwala, S.R., Halpern, M., Hasselfield, M., Hildebrandt, S.R., Hilton, G.C., Hristov, V., Hui, H., Irwin, K.D., Jones, W.C., Karkare, K.S., Kaufman, J.P., Keating, B.G., Kefeli, S., Kernasovskiy, S.A., Kovac, J.M., Kuo, C.L., LeDuc, H.G., Leitch, E.M., Llombart, N., Lueker, M., Mason, P., Megerian, K., Moncelsi, L., Netterfield, C.B., Nguyen, H.T., O'Brient, R., Ogburn, I. R. W., Orlando, A., Pryke, C., Rahlin, A.S., Reintsema, C.D., Richter, S., Runyan, M.C., Schwarz, R., Sheehy, C.D., Staniszewski, Z.K., Sudiwala, R.V., Teply, G.P., Tolan, J.E., Trangsrud, A., Tucker, R. S., Turner, A.D., Vieregg, A.G., Weber, A., Wiebe, D.V., Wilson, P., Wong, C.L., Yoon, K.W., Zmuidzinas, J.: Antenna-coupled TES Bolometers Used in BICEP2, Keck Array, and Spider. Apj **812** (2), 176 (2015) https://doi.org/10.1088/0004-637X/812/2/176arXiv:1502.00619 [astro-ph.IM]

3. ...A. Suzuki, P. Ade, Y. Akiba, C. Aleman, K. Arnold, C. Baccigalupi, B. Barch, D. Barron, A. Bender, D. Boettger, J. Borrill, S. Chapman, Y. Chinone, A. Cukierman, M. Dobbs, A. Ducout, R. Dunner, T. Elleflot, J. Errard, G. Fabbian, S. Feeney, C. Feng, T. Fujino, G. Fuller, A. Gilbert, N. Goeckner-Wald, J. Groh, T.D. Haan, G. Hall, N. Halverson, T. Hamada, M. Hasegawa, K. Hattori, M. Hazumi, C. Hill, W. Holzapfel, Y. Hori, L. Howe, Y. Inoue, F. Irie, G. Jaehnig, A. Jaffe, O. Jeong, N. Katayama, J. Kaufman, K. Kazemzadeh, B. Keating, Z. Kermish, R. Keskitalo, T. Kisner, A. Kusaka, M.L. Jeune, A. Lee, D. Leon, E. Linder, L. Lowry, F. Matsuda, T. Matsumura, N. Miller, K. Mizukami, J. Montgomery, M. Navaroli, H. Nishino, J. Peloton, D. Poletti, G. Puglisi, G. Rebeiz, C. Raum, C. Reichardt, P. Richards, C. Ross, K. Rotermund, Y. Segawa, B. Sherwin, I. Shirley, P. Siritanasak, N. Stebor, R. Stompor, J. Suzuki, O. Tajima, S. Takada, S. Takakura, S. Takatori, A. Tikhomirov, T. Tomaru, B. Westbrook, N. Whitehorn, T. Yamashita, A. Zahn, O. Zahn, The polarbear-2 and the simons array experiments. J. Low Temp. Phys. **184**(3–4), 805–810 (2016). https://doi.org/10.1007/s10909-015-1425-4

4. Galitzki, N., Baildon, T., Barron, D., Lashner, J., Lee, A.T., Li, Y., Limon, M., Lungu, M., Matsuda, F., Mauskopf, P.D., May, A.J., McCallum, N., McMahon, J., Nati, F., Niemack, M.D., Orlowski-Scherer, J.L., Parshley, S.C., Piccirillo, L., Rao, M.S., Salatino, M., Seibert, J.S., Sierra, C., Silva-Feaver, M., Simon, S.M., Staggs, S.T., Stevens, J.R., Suzuki, A., Teply, G., Thornton, R., Tsai, C., Ullom, J.N., Vavagiakis, E.M., Vissers, M.R., Westbrook, B., Wollack, E.J., Xu, Z., Zhu, N., Raum, C., Beckman, S., Jeong, O., Ali, A., Arnold, K.S., Ashton, P.C., Austermann, J.E., Baccigalupi, C., Beall, J.A., Bruno, S.M.M., Bryan, S., Calisse, P.G., Chesmore, G.E., Chinone, Y., Choi, S.K., Coppi, G., Crowley, K.D., Crowley, K.T., Cukierman, A., Devlin, M.J., Dicker, S., Dober, B., Duff, S.M., Dunkley, J., Fabbian, G., Gallardo, P.A., Gerbino, M., Goeckner-Wald, N., Golec, J.E., Gudmundsson, J., Healy, E.E., Henderson, S., Hill, C.A., Hilton, G.C., Ho, S.-P.P., Howe, L.A., Hubmayr, J., Keating, B., Koopman, B.J., Kuichi, K., Kusaka, A.: The simons observatory: instrument overview. In: Zmuidzinas, J., Gao, J.-R. (eds.) Millimeter, Submillimeter, and Far-Infrared Detectors and Instrumentation for Astronomy IX. SPIE, ??? (2018). https://doi.org/10.1117/12.2312985

5. Abazajian, K., Abdulghafour, A., Addison, G.E., Adshead, P., Ahmed, Z., Ajello, M., Akerib, D., Allen, S.W., Alonso, D., Alvarez, M., Amin, M.A., Amiri, M., Anderson, A., Ansarinejad, B., Archipley, M., Arnold, K.S., Ashby, M., Aung, H., Baccigalupi, C., Baker, C., Bakshi, A., Bard, D., Barkats, D., Barron, D., Barry, P.S., Bartlett, J.G., Barton, P., Basu Thakur, R., Battaglia, N., Beall, J., Bean, R., Beck, D., Belkner, S., Benabed, K., Bender, A.N., Benson, B.A., Besuner, B., Bethermin, M., Bhimani, S., Bianchini, F., Biquard, S., Birdwell, I., Bischoff, C.A., Bleem, L., Bocaz, P., Bock, J. J., Bocquet, S., Boddy, K.K., Bond, J.R., Borrill, J., Bouchet, F.R., Brinckmann, T., Brown, M.L., Bryan, S., Buza, V., Byrum, K., Calabrese, E., Calafut, V., Caldwell, R., Carlstrom, J.E., Carron, J., Cecil, T., Challinor, A., Chan, V., Chang, C.L., Chapman, S., Charles, E., Chauvin, E., Cheng, C., Chesmore, G., Cheung, K., Chinone, Y., Chluba, J., Cho, H.-M.S., Choi, S., Clancy, J., Clark, S.,

Cooray, A., Coppi, G., Corlett, J., Coulton, W., Crawford, T.M., Crites, A., Cukierman, A., Cyr-Racine, F.-Y., Dai, W.-M., Daley, C., Dart, E., Daues, G., de Haan, T., Deaconu, C., Delabrouille, J., Derylo, G., Devlin, M., Di Valentino, E., Dierickx, M., Dober, B., Doriese, R., Duff, S., Dutcher, D., Dvorkin, C., Dünner, R., Eftekhari, T., Eimer, J., El Bouhargani, H., Elleflot, T., Emerson, N., Errard, J., Essinger-Hileman, T., Fabbian, G., Fanfani, V., Fasano, A., Feng, C., Ferraro, S., Filippini, J.P., Flauger, R., Flaugher, B., Fraisse, A.A., Frisch, J., Frolov, A., Galitzki, N., Gallardo, P.A., Galli, S., Ganga, K., Gerbino, M., Giannakopoulos, C., Gilchriese, M., Gluscevic, V., Goeckner-Wald, N., Goldfinger, D., Green, D., Grimes, P., Grin, D., Grohs, E., Gualtieri, R., Guarino, V., Gudmundsson, J. E., Gullett, I., Guns, S., Habib, S., Haller, G., Halpern, M., Halverson, N.W., Hanany, S., Hand, E., Harrington, K., Hasegawa, M., Hasselfield, M., Hazumi, M., Heitmann, K., Henderson, S., Hensley, B., Herbst, R., Hervias-Caimapo, C., Hill, J.C., Hills, R., Hivon, E., Hlozek, R., Ho, A., Holder, G., Hollister, M., Holzapfel, W., Hood, J., Hotinli, S., Hryciuk, A., Hubmayr, J., Huffenberger, K.M., Hui, H., Ibá nez, R., Ibitoye, A., Ikape, M., Irwin, K., Jacobus, C., Jeong, O., Johnson, B.R., Johnstone, D., Jones, W.C., Joseph, J., Jost, B., Kang, J.H., Kaplan, A., Karkare, K.S., Katayama, N., Keskitalo, R., King, C., Kisner, T., Klein, M., Knox, L., Koopman, B.J., Kosowsky, A., Kovac, J., Kovetz, E.D., Krolewski, A., Kubik, D., Kuhlmann, S., Kuo, C.-L., Kusaka, A., Lähteenmäki, A., Lau, K., Lawrence, C.R., Lee, A.T., Legrand, L., Leitner, M., Leloup, C., Lewis, A., Li, D., Linder, E., Liodakis, I., Liu, J., Long, K., Louis, T., Loverde, M., Lowry, L., Lu, C., Lubin, P., Ma, Y.-Z., Maccarone, T., Madhavacheril, M.S., Maldonado, F., Mantz, A., Marques, G., Matsuda, F., Mauskopf, P., May, J., McCarrick, H., McCracken, K., McMahon, J., Meerburg, P.D., Melin, J.-B., Menanteau, F., Meyers, J., Millea, M., Miranda, V., Mitchell, D., Mohr, J., Moncelsi, L., Monzani, M.E., Moshed, M., Mroczkowski, T., Mukherjee, S., Münchmeyer, M., Nagai, D., Nagarajappa, C., Nagy, J., Namikawa, T., Nati, F., Natoli, T., Nerval, S., Newburgh, L., Nguyen, H., Nichols, E., Nicola, A., Niemack, M.D., Nord, B., Norton, T., Novosad, V., O'Brient, R., Omori, Y., Orlando, G., Osherson, B., Osten, R., Padin, S., Paine, S., Partridge, B., Patil, S., Petravick, D., Petroff, M., Pierpaoli, E., Pilleux, M., Pogosian, L., Prabhu, K., Pryke, C., Puglisi, G., Racine, B., Raghunathan, S., Rahlin, A., Raveri, M., Reese, B., Reichardt, C.L., Remazeilles, M., Rizzieri, A., Rocha, G., Roe, N.A., Rotermund, K., Roy, A., Ruhl, J.E., Saba, J., Sailer, N., Salatino, M., Saliwanchik, B., Sapozhnikov, L., Sathyanarayana Rao, M., Saunders, L., Schaan, E., Schillaci, A., Schmitt, B., Scott, D., Sehgal, N., Shandera, S., Sherwin, B.D., Shirokoff, E., Shiu, C., Simon, S.M., Singari, B., Slosar, A., Spergel, D., St. Germaine, T., Staggs, S.T., Stark, A.A., Starkman, G.D., Steinbach, B., Stompor, R., Stoughton, C., Suzuki, A., Tajima, O., Tandoi, C., Teply, G.P., Thayer, G., Thompson, K., Thorne, B., Timbie, P., Tomasi, M., Trendafilova, C., Tristram, M., Tucker, C., Tucker, G., Umiltà, C., van Engelen, A., van Marrewijk, J., Vavagiakis, E.M., Vergès, C., Vieira, J.D., Vieregg, A.G., Wagoner, K., Wallisch, B., Wang, G., Wang, G.-J., Watson, S., Watts, D., Weaver, C., Wenzl, L., Westbrook, B., White, M., Whitehorn, N., Wiedlea, A., Williams, P., Wilson, R., Winch, H., Wollack, E.J., Kimmy Wu, W.L., Xu, Z., Yefremenko, V.G., Yu, C., Zegeye, D., Zivick, J., Zonca, A.: Snowmass 2021 CMB-S4 White Paper. arXiv e-prints, 2203–08024 (2022) https://doi.org/10.48550/arXiv.2203.08024arXiv:2203.08024 [astro-ph.CO]

6. S.W. Henderson, R. Allison, J. Austermann, T. Baildon, N. Battaglia, J.A. Beall, D. Becker, F. De Bernardis, J.R. Bond, E. Calabrese, S.K. Choi, K.P. Coughlin, K.T. Crowley, R. Datta, M.J. Devlin, S. M. Duff, J. Dunkley, R. Dünner, A. van Engelen, P.A. Gallardo, E. Grace, M. Hasselfield, F. Hills, G. C. Hilton, A.D. Hincks, R. Hložek, S.P. Ho, J. Hubmayr, K. Huffenberger, J.P. Hughes, K.D. Irwin, B. J. Koopman, A.B. Kosowsky, D. Li, J. McMahon, C. Munson, F. Nati, L. Newburgh, M.D. Niemack, P. Niraula, L.A. Page, C.G. Pappas, M. Salatino, A. Schillaci, B.L. Schmitt, N. Sehgal, B.D. Sherwin, J.L. Sievers, S.M. Simon, D.N. Spergel, S.T. Staggs, J.R. Stevens, R. Thornton, J. Van Lanen, E.M. Vavagiakis, J.T. Ward, E.J. Wollack, Advanced ACTPol cryogenic detector arrays and readout. J. Low Temp. Phys. **184**(3–4), 772–779 (2016). https://doi.org/10.1007/s10909-016-1575-z. arXiv:1510.02809 [astro-ph.IM]
7. Li, H., Li, S.-Y., Liu, Y., Li, Y.-P., Cai, Y., Li, M., Zhao, G.-B., Liu, C.-Z., Li, Z.-W., Xu, H., Wu, D., Zhang, Y.-J., Fan, Z.-H., Yao, Y.-Q., Kuo, C.-L., Lu, F.-J., Zhang, X.: Probing primordial gravitational waves: Ali CMB polarization telescope. arXiv e-prints, 1710–03047 (2017) https://doi.org/10.48550/arXiv.1710.03047arXiv:1710.03047 [astro-ph.CO]
8. D. Li, J.E. Austermann, J.A. Beall, D.T. Becker, S.M. Duff, P.A. Gallardo, S.W. Henderson, G.C. Hilton, S.-P. Ho, J. Hubmayr, B.J. Koopman, J.J. McMahon, F. Nati, M.D. Niemack, C.G. Pappas, M. Salatino, B.L. Schmitt, S.M. Simon, S.T. Staggs, J. Van Lanen, J.T. Ward, E.J. Wollack, AlMn transition edge sensors for advanced ACTPol. J. Low Temp. Phys. **184**(1–2), 66–73 (2016). https://doi.org/10.1007/s10909-016-1526-8

9. A. Suzuki, E. Kane, A.T. Lee, T. Liu, C. Raum, M. Renzullo, P. Truitt, J. Vivalda, B. Westbrook, D. Yohannes, Recent developments of commercially fabricated horn antenna-coupled transition-edge sensor bolometer detectors for next-generation cosmic microwave background polarimetry experiments. J. Low Temp. Phys. **209**(5–6), 1111–1118 (2022). https://doi.org/10.1007/s10909-022-02731-x
10. X. Qian, N. Parson, X.-G. Chen, Effects of mn content on recrystallization resistance of aa6082 aluminum alloys during post-deformation annealing. J. Mater. Sci. Technol. **52**, 189–197 (2020). https://doi.org/10.1016/j.jmst.2020.04.015
11. Westbrook, B.e.a.: The POLARBEAR-2 and Simons Array Focal Plane Fabrication Status. J. Low Temp. Phys. **193**(5-6), 758–770 (2018) https://doi.org/10.1007/s10909-018-2059-0arXiv:2210.04117 [astro-ph.IM]
12. Westbrook, B., Raum, C., Beckman, S., Lee, A.T., Farias, N., Sasse, T., Suzuki, A., Kane, E., Austermann, J.E., Beall, J.A., Duff, S.M., Hubmayr, J., Hilton, G.C., Lanen, J.V., Vissers, M.R., Link, M.R., Halverson, N., Jaehnig, G., Ghinga, T., Stever, S., Minami, Y., Thompson, K.L., Russell, M., Arnold, K., Seibert, J., Silva-Feaver, M.: Detector fabrication development for the LiteBIRD satellite mission. In: Lystrup, M., Perrin, M.D., Batalha, N., Siegler, N., Tong, E.C. (eds.) Space Telescopes and Instrumentation 2020: Optical, Infrared, and Millimeter Wave, vol. 11443, p. 114435. SPIE, ??? (2020). https://doi.org/10.1117/12.2562978 . International Society for Optics and Photonics

Authors and Affiliations

Benjamin Westbrook[1] · Bhoomija Prasad[1] · Christopher R. Raum[1] · Adrian T. Lee[1] · Aritoki Suzuki[2] · Johannes Hubmayr[3] · Shannon M. Duff[3] · Micheal J. Link[3] · Tammy J. Lucas[3]

✉ Benjamin Westbrook
bwestbrook@berkeley.edu

[1] Department of Physics, University of California, Berkeley, 151 Physics North, Berkeley, CA 94720, USA

[2] Physics Division, Lawrence Berkeley National Laboratory, 1 Cyclotron Road, Berkeley, CA 94720, USA

[3] National Institute of Standards and Technology, 325 Broadway, Boulder, CO 80305, USA